Title

Biofabricated Soft Network Composites for Cartilage Tissue Engineering

Authors list and affiliations

Onur Bas[1], Elena M. De-Juan-Pardo[1], Christoph Meinert[1], Davide D'Angella[2], Jeremy G. Baldwin[1], Laura J. Bray[1], R. Mark Wellard[3], Stefan Kollmannsberger[4], Ernst Rank[2], Carsten Werner[5], Travis J. Klein[1,6], Isabelle Catelas[3,7], and Dietmar W. Hutmacher[1,2,6]*

*Corresponding author

Email: dietmar.hutmacher@qut.edu.au

[1] Institute of Health and Biomedical Innovation, Centre for Regenerative Medicine, Queensland University of Technology (QUT), Musk Avenue, Kelvin Grove, Brisbane, QLD 4059, Australia

[2] Institute for Advanced Study, Technische Universität München, Lichtenbergstraße 2 a, 85748 Garching, Germany

[3] School of Chemistry, Physics and Mechanical Engineering, Science and Engineering Faculty, Queensland University of Technology, Brisbane, QLD 4001, Australia

[4] Chair for Computation in Engineering, Technische Universität München, D-80333, Munich, Germany

[5] Leibniz Institute of Polymer Research Dresden Hohe Straße 6, 01069 Dresden, Saxony, Germany

[6] ARC Training Centre In Additive Biomanufacturing, Queensland University of Technology, Musk Avenue, Kelvin Grove, Brisbane, QLD 4059, Australia

[7] Department of Mechanical Engineering, University of Ottawa, Ottawa, ON, Canada

Abstract

Articular cartilage from a material science point of view is a soft network composite that plays a critical role in load-bearing joints during dynamic loading. Its composite structure, consisting of a collagen fiber network and a hydrated proteoglycan matrix, gives rise to the complex mechanical properties of the tissue including viscoelasticity and stress relaxation. Melt Electrospinning Writing (MEW) allows the design and fabrication of medical grade polycaprolactone (mPCL) fibrous networks for the reinforcement of soft hydrogel matrices for cartilage tissue engineering. However, these fiber-reinforced constructs underperformed under dynamic and prolonged loading conditions, suggesting that more targeted design approaches and material selection are required to fully exploit the potential of fibers as reinforcing agents for cartilage tissue engineering. In this study, we emulate the proteoglycan matrix of articular cartilage by using highly negatively charged star-shaped poly(ethylene glycol)/heparin hydrogel (sPEG/Hep) as the soft matrix. These soft hydrogels combined with mPCL melt electrospun fibrous networks exhibit mechanical anisotropy, nonlinearity, viscoelasticity and morphology analogous to those of their native counterpart, and provide suitable microenvironment for *in vitro* human chondrocyte culture and neocartilage formation. In addition, a high-order finite element methods (p-FEM) was developed in order to gain further insights concerning the deformation mechanisms of the constructs *in silico* as well as to predict compressive moduli. To our knowledge, this is the first study presenting cartilage tissue-engineered constructs that capture the overall transient, equilibrium and dynamic biomechanical properties of human articular cartilage.

Keywords

biomimetics, hydrogels, fiber reinforcement, tissue engineering, articular cartilage, melt electrospinning writing, soft fibrous network composites

1 Introduction

Nature transforms individually weak materials into high performance composites and hence, hard and soft structural biomaterials found in nature have spurred motivation for the design of materials with biomimetic properties [1–3]. Blueprints of nature's hard structural materials such as bone, dentine and nacre have been widely applied to engineer new innovative materials [4–7]. Yet, the combination of a bioinspired and a biomimetic strategy to create advanced soft network composites has remained largely unexplored.

Fibers are the basic structural building blocks of many soft matrix tissues [8]. Heart valve, skin, intervertebral disc and articular cartilage are formed by stiff and strong collagen fibrils interspersed among a weak extracellular matrix (ECM). In addition to structural integrity, fibers can bring anisotropy and depth-dependent mechanical properties to natural materials with their orientation and density gradient [9,10]. Despite their fundamental role in natural tissues, it is only recently that a particular emphasis in the Tissue Engineering and Regenerative Medicine (TE & RM) community has been placed on fiber-reinforced hydrogels. Bio-textile substrates [11,12], solution electrospun [13,14] and non-woven [15] meshes have been incorporated with soft hydrogels for mechanical enhancement. However, the high fiber content, the limited architectural arrangement of fibers and low interconnected porosity, as well as the thickness in the resulting composites remain major drawbacks to fulfil the biological requirements for many TE & RM applications. To address these drawbacks, we recently introduced a reinforcement strategy for soft matrices in which hydrogels were strengthened with fibrous networks manufactured by means of Melt Electrospinning Writing (MEW) technology [16,17]. Results showed up to a 54-fold increase in the compressive modulus of these composite constructs, with the mesh only contributing less than 10 percentage of the construct volume [16,17]. However, fiber-reinforced constructs underperformed under dynamic and prolonged loading

conditions, suggesting that more targeted design approaches and material selection are required to fully exploit the potential of fibers as reinforcing agents for cartilage tissue engineering.

In this study, we aimed to develop enhanced fiber-reinforced hydrogels that could resemble the overall complex mechanical properties of the cartilage, including viscoelasticity and stress relaxation. We hypothesized that these unique features could only be achieved by carefully selecting a hydrogel that emulates the negatively charged proteoglycan matrix of articular cartilage. In order to do so, we chose star-shaped poly(ethylene glycol)/heparin hydrogel (sPEG/Hep) as the soft matrix. sPEG/Hep hydrogels are a bio-hybrid gel system consisting of a thiol-end modified star-shaped poly(ethylene glycols) (PEG) and negatively charged maleimide-functionalized heparin, cross-linked via a Michael addition reaction [18]. These hydrogels have a broad range of applications in TE & RM [19–23]. Along with sPEG/Hep, we have used fibrin gel as the second biomaterial in this study. Fibrin is a natural polymeric protein which is involved in critical blood coagulation processes. It is formed by fibrinogen, a plasma protein, when activated by the enzyme thrombin [24]. It has been implemented for engineering various tissues, including articular cartilage [25,26]. Therefore, fibrin was considered as a suitable control material for the study. mPCL melt electrospun fibrous networks with different architectures were additive biomanufactured via MEW to reinforce these soft sPEG/Hep hydrogels.

Mechanical tests were performed alongside a benchmark of native human articular cartilage and the reinforcement concept was further investigated using high-order finite element methods (p-FEM). Last, human articular chondrocytes were encapsulated and cultured for 14 days in fiber-reinforced sPEG/Hep in the presence and absence of mechanical loading to examine the *in vitro* performance of the constructs. To our knowledge, this is the first study presenting cartilage tissue-engineered constructs that capture the overall transient, equilibrium and dynamic biomechanical properties of human articular cartilage.

2 Materials and methods

2.1 Biofabrication of fiber-reinforced hydrogel composites

MEW, a technology combining additive manufacturing and electrospinning principles, was employed to manufacture the reinforcing fibrous networks, as described in detail elsewhere [27] (the schematic illustration of the device and the printing parameters are depicted in Figure 1a). Briefly, molten mPCL (100 Cº) was extruded through a 23G needle at a volumetric flow rate of 20 µl h^{-1}. A high voltage of 12.0 – 12.5 kV was applied to the needle. Generated fine polymeric jet was collected on an aluminum collector plate at a translational velocity of 0.7 m min^{-1} in a layer-by-layer manner using a motorized X-Y stage controlled with a computer. Nozzle-to-collector distance was kept at 15.0 mm.

200, 400 and 600 µm pore-sized fibrous networks were printed with a laydown pattern of 0° – 90° (50 mm x 50 mm x 1.5 mm), pre-programmed in G code. We have previously shown that fibrous networks having a pore-size within this range provide reinforcement effect to capture the transient mechanical properties of the native tissues [16,17]. These fibrous networks were then cut into 5.0 mm diameter round samples using a laser-cutting machine equipped with a 75 W laser (ILS12.75, Universal Laser Systems, Inc. USA). A 7.5 W cutting power and 800 dots per inch (DPI) of dot density settings were used for the cutting process. The surface of the fibers was then modified in order to increase their wettability [28]. The laser-cut samples were immersed into a pre-heated 2.5 M NaOH (37 °C) for 30 mins. For uniform treatment, first, the samples in the solution were placed into a vacuum chamber for 5 min to remove the entrapped air bubbles. The rest of the etching process was carried out in a 37 °C incubator. Samples were then rinsed in double-distilled water several times to remove NaOH residues and reach pH 7, and finally dried overnight in a vacuum desiccator at room temperature. Wettability was evaluated by performing contact angle measurements (FTA200, Poly-Instruments Pty. Ltd.,

Australia) on treated and untreated fibrous networks with 200-µm fiber spacing (n=3 for each group) (Figure S1).

Polymer-peptide conjugates for sPEG/Hep hydrogels were prepared as previously described [18]. Briefly, four-armed maleimide terminated poly(ethylene glycol) (PEG-Mal; Mn = 10.0x103; PDI = 1.08) was purchased from JenKem Technology USA Inc. (Allen, USA). All four arms were then conjugated to an MMP-cleavable peptide synthesised in-house. Heparin, sodium salt, porcine intestinal mucosa (14,000 g/mol) was purchased from Merck Millipore, (Darmstadt, Germany) and conjugated with six maleimide groups per heparin molecule in-house. Subsequently, hydrogels with a molar ratio (γ) of 1.5, 3.36 mg of heparin-maleimide conjugate (MW = 15,000) and 5.35 mg of PEG-$(MMP)_4$ conjugate (MW = 15,920) were each re-suspended in 75 µL of phosphate buffered saline (PBS). The solutions were mixed at a ratio of 1:1. Fibrin was prepared by polymerization of a 72-110 mg mL^{-1} human fibrinogen solution with a 2 IU mL^{-1} human thrombin solution (Artiss, Baxter AG, Austria) (1:1 volume ratio). The 2 IU mL^{-1} thrombin solution was prepared from a 4 IU mL^{-1} solution diluted in 40 mM Calcium Chloride ($CaCl_2$). This concentration was previously tested to optimize the clotting time of fibrin during the injection molding process. All precursor hydrogel solutions were gently mixed to ensure homogeneity and subsequently centrifuged to remove any air bubbles. A positive displacement pipette was used to inject freshly prepared hydrogel precursor solutions into the wells of a custom-made injection mold (5.0 mm diameter and 1.0 mm height), with or without a fibrous network (Figure 1e). The mold was kept at 37 C° for 30 min to ensure crosslinking. Samples were stored in Dulbecco's Modified Eagle Medium (DMEM) (Sigma Aldrich) in a humidified incubator at 37 °C and 5% CO_2, and allowed to swell for 24 to 32 h before evaluation.

2.2 Morphological characterization

Field Emission Scanning Electron Microscope (FE-SEM; Carl Zeiss Microscopy GmbH, Germany) was used to analyze the fibrous network morphology and to quantify the diameter of the fibers. Diameter measurements were conducted on FE-SEM micrographs of the fibrous networks by analyzing randomly selected fibers (n=50) using ImageJ (National Institutes of Health, USA). The general morphology of the hydrogel and fiber-reinforced hydrogel constructs was evaluated under a stereomicroscope (Leica M125, Leica Microsystems, Germany) to investigate the structural order of the fibrous networks in the hydrogels, the quality of the hydrogel infiltration, and the presence of any air pockets. Additional magnetic resonance micro-imaging was performed on non-translucent fibrin-based samples (n=3) using a 300 MHz Bruker Avance magnetic resonance spectrometer equipped with a 7.0 Tesla magnet and micro120 imaging gradients (Bruker, Germany) for the same purpose (Figure S2). T2-weighted images were acquired using an MSME pulse sequence at 256 x 256 µm in-plane resolution, 16 averages, and a field of view of 10 mm using 7.0 ms echo and 1000.0 ms repetition time settings.

2.3 Estimation of volumetric hydrogel fraction of fiber-reinforced hydrogel constructs

The hydrogel content of the fiber-reinforced hydrogels was determined volumetrically. The weight of the fibrous networks was first measured using a microbalance and then used to calculate the true fibrous network volume for each sample ($Volume_{Fibrous\ networks} = Mass_{Fibrous\ networks} / Density_{mPCL}$), ($Density_{mPCL}$ = 1.145 g cm^{-3}), (n=30). It was assumed that the pores of the fibrous networks and the remainder of the mold space (5.0 mm diameter and 1.0 mm height) were completely filled with hydrogel. The volumetric hydrogel fraction of the final composites was therefore estimated using the following equation:

$$\text{Volumetric hydrogel fraction (\%)} = \left(\frac{V_{Mould} - V_{Fibrous\ networks}}{V_{Mould}}\right) \text{x } 100) \quad (1)$$

Since this formula does not take into account the swelling of the hydrogels, the calculated values indicate the theoretical hydrogel fraction of the constructs immediately after the molding process.

2.4 Mechanical testing and analysis

All mechanical tests were carried out in an unconfined compression arrangement on a custom-made platform using an Instron MicroTester fitted with a 5 N load cell (5848, Instron, Australia). The platform had a glass bottom with a calibration scale bar and was equipped with a digital microscope camera underneath to capture images from below. Samples were completely submerged in DMEM at 37 °C during the tests to prevent their dehydration and to simulate a physiological environment. A compressive strain of ~30% of the construct height was applied at a displacement rate of 0.01 mm s^{-1}, and the compressive modulus (E) was determined from the slope of the linear region of the stress vs. strain plots between 10-15% strain (n=6). Stepwise stress-relaxation tests were performed to evaluate the equilibrium behavior of the samples (n=4). First, a 0.01 N tare load was applied. The samples were then subjected to 5% ramp compressive strain steps, each followed by a relaxation period (600 s for hydrogels; fiber-reinforced hydrogels and articular cartilage; and 300 s for fibrous networks alone), to a total of 20% strain. Stress-relaxation criterion was <10 Pa s^{-1}. The stress-relaxation curves of the samples which haven't relaxed in the given time were extrapolated until they met the stress-relaxation criterion set. A two-phase exponential decay function was used to fit the curves ($R^2 > 0.999$) and for the extrapolation (GraphPad v6.05, USA). Stress/strain curves of the relaxation points were plotted, and the slope was used to determine the equilibrium modulus ($E_{Eq.}$). Images of the samples were captured at the beginning (0% strain) and the end (20% strain) of the stress-relaxation tests. The images were then processed with ImageJ to quantify the lateral dimensional changes of the samples in response to the axial compression to calculate Poisson's ratio (v) in equilibrium. At the end of the stress-relaxation tests, samples were

subjected to one hundred cycles of a sinusoidal compressive strain at a 2.5% amplitude and a frequency of 0.1 Hz. Dynamic mechanical properties of the samples (storage (E') and loss (E'') moduli, as well as loss factor (E''/E')) were evaluated at the last compression cycle using the viscoelastic theory, with σ_0 and ε_0 being the amplitudes of stress and strain, respectively, and δ the phase shift [29].

$$\left(E' = \frac{\sigma_0}{\varepsilon_0}\cos\delta\right) \quad (2)$$

$$\left(E'' = \frac{\sigma_0}{\varepsilon_0}\sin\delta\right) \quad (3)$$

Articular cartilage samples were treated similarly (n=6 for uniaxial compression test, n= 4 stepwise stress-relaxation test followed by dynamic mechanical test). Articular cartilage was obtained with institutional ethics approval from consenting patients undergoing total knee replacement surgeries for osteoarthritis. Full-thickness cartilage explants were harvested from macroscopically healthy areas of the lateral femoral condyle (diameter = 5 mm, height = ~1.2 – 2.0 mm) of one donor (71-year old male).

Mechanical properties of NaOH-treated fibers were investigated with tensile tests. Due the limited resolution of the available load cell (5N) to test very fine fibers, thirty of these fibers were printed in a wall-like shape for testing instead of being tested individually (Figure S3). To ease the handling, the fibers were secured within a cardboard frame [30]. Tensile tests were conducted by pulling the fibers at a displacement rate of 0.01 mm s^{-1} using an Instron MicroTester (n=10).

2.5 Measurement of the water release rate from hydrogels in compression tests

The water retention ability of the hydrated hydrogels under a compressive load was evaluated using a similar loading protocol applied for testing the compressive modulus of the samples (20% total strain, 0.01 mm s^{-1}). In contrast, however, this test was performed in air, allowing

the collection of the extruded fluid from hydrogels on the testing platform after compression. The extruded fluid around the compressed samples was collected using low lint content wipers (KimWipe) before releasing the compression to prevent potential water reuptake. Tested samples were put into pre-weighed tubes to prevent the samples from losing weight due to evaporation. The weight of the hydrogels before and after compression was compared to determine the amount of water lost.

2.6 Equilibrium partitioning of an ionic contrast agent-microcomputed tomography (EPIC-μCT)

An EPIC-μCT study was performed to investigate the negative charge density of the hydrogels. Specimens were immersed in a mixture of 40% (v/v) ioxaglate (Hexabrix, Aspen, Australia) in DMEM at room temperature on a rocker for 12 h. Samples were then imaged in a μCT 40 scanner (Scanco Medical, Brüttisellen, Switzerland) and processed using the Scanco μCT software [31]. Gray scale images from the EPIC-μCT scans were processed with ImageJ to quantify the means of the gray values in the images (Figure S4).

2.7 Simulations

The numerical experiments were conducted by using the p-version of the finite element method (p-FEM) on hexahedral elements. Both of the constituents of the models were assumed to be isotropic, behave linearly, and deform elastically. In the computational mesh, each fiber was modelled by three elements forming a solid with an octagonal cross-sectional surface, while the hydrogel was modelled by elements filling the space between the fibers. The element maximum and minimum lengths were associated to the fibrous network pore size and fiber diameter, respectively. The p-FEM method has been shown to be suitable for such elements with high aspect ratio [32]. A linear-elastic material model was adopted in the present study. The material parameters (compressive modulus (E) and Poisson's ratio (ν)) were assigned to each fiber- and hydrogel-element. Experimental data were used as the input for the simulations: $E_{sPEG/Hep}$ =

34.99 kPa; E_{mPCL} = 317.18 MPa. Poisson's ratio of sPEG/Hep was measured to be 0.45 ± 0.03 in the stress relaxation tests. However, since the purpose of the simulations was to measure the stiffness of the constructs at rapid loading, it was assumed that there was not enough time for the water to leave the hydrogel. Therefore, 0.495 was assigned for the *v* value of hydrogel phase while considering that the hydrogel behaves as an almost incompressible material when loaded at high strain rates. Poisson's ratio of bulk mPCL was defined as 0.3. Idealized models of constructs were tested in the simulations. Models consisted of 24x24, 12x12 or 8x8 pore units for the 200-µm, 400-µm or 600-µm pore size fibrous networks, respectively.

The fiber-elements share the face associated to other fiber contact surfaces, resulting in an infinite-strength fiber to fiber bonding. Since the fibrous networks consist of repeating units in z-direction, two layers of fibers were simulated. Moreover, the symmetry of the fibrous networks allowed simulating only one quarter of the geometry. Therefore, we imposed symmetry boundary conditions on the symmetry faces of the model to reduce computational cost. The compression was enforced by a strong Dirichlet boundary condition on the bottom face while the remaining faces were subjected to a homogeneous Neumann boundary condition. This simplified model represented the entire geometry. The compressive modulus (*E*) was computed from the extrapolated internal energy of the system. Namely, the exact internal energy was approximated by extrapolation of a sequence of internal energies obtained by p-extension, as described in detail elsewhere [33].

2.8 In vitro testing

2.8.1 Cartilage explant preparation, chondrocyte isolation and expansion culture

Articular chondrocytes were isolated from macroscopically normal full-thickness cartilage of a 67-year old male donor based on a protocol previously described [34]. All human articular

cartilage explants were collected with patient consent and ethical approval from the Prince Charles Hospital and Queensland University of Technology (Ethics RM: 1400001024).

Cells were propagated on tissue culture plastic dishes (seeded at 3000 cells cm^{-2}) in low-D-glucose chondrocyte basal medium (DMEM with 2 mM GlutaMAX™, 10 mM 4-(2-hydroxyethyl)-1-piperazineethanesulfonic acid (HEPES), 0.1 mM nonessential amino acids, 50 U mL^{-1} penicillin, 50 µg mL^{-1} streptomycin, and 0.5 µg mL^{-1} amphotericin B (Fungizone®) (all from Invitrogen, CA, USA), 0.4 mM L-proline and 0.1 mM L-ascorbic acid (both from Sigma-Aldrich), supplemented with 10% fetal bovine serum (FBS) (Hyclone, Logan, UT, USA). All cells and cell/hydrogel constructs were maintained at 37 °C in a humidified 5% CO_2/95% air CO_2 incubator and the culture medium changed every 3-4 days.

Passage 1 human articular chondrocytes were encapsulated in sPEG/Hep with and without melt electrospun fibrous networks by first re-suspending the cells in the hydrogel precursor solution at 10 million cells mL^{-1}. In order to benefit from the superior biological properties of the hydrogel [20,35], we have chosen composites reinforced with 600µm pore-sized fibrous networks for our preliminary in vitro study, which presented the highest volumetric hydrogel fraction among our samples. Cell/hydrogel constructs with and without the fibrous networks were cultured in serum-free high-D-glucose basal chondrocyte medium (see above for composition) with ITS-G (100 × dilution), 1.25 mg ml^{-1} bovine serum albumin (BSA), 0.1 µM dexamethasone (all Sigma-Aldrich) and 10 ng ml^{-1} transforming growth factor beta 3 (TGF-β3) (GroPep, Adelaide, SA, Australia).

2.8.2 Cell Viability Assay

At days 1 and 14 of culture, live and dead cells were visualized with fluorescein diacetate (FDA) and propidium iodide (PI) (both Sigma-Aldrich), respectively. Cell/hydrogel constructs were washed in PBS, incubated in a solution containing 10 µg ml^{-1} FDA and 5 µg ml^{-1} PI in PBS for

5 min at room temperature, and then washed in PBS again. Images were captured using a Carl Zeiss fluorescence microscope, and the percentage of viable cells was determined using ImageJ software (National Institutes of Health, USA).

2.8.3 Biaxial mechanical stimulation and gene expression analysis

Constructs were pre-cultured under free swelling conditions for 14 days to allow for chondrocyte re-differentiation and formation of a protective pericellular matrix [34] before mechanical stimulation. Unconfined biaxial mechanical stimulation was carried out in a custom shear and compression bioreactor system housed in an incubator. Loading was facilitated by polytetrafluoroethylene (PTFE) plungers driven by two orthogonally aligned micro linear actuators (T-NA Micro Linear Actuators, Zaber Technologies, Vancouver, Canada) with a resolution of < 50 nm and a repeatability of < 1 µm. Constructs were dynamically loaded for 1 h at 1 Hz at a compressive strain of ~ 20% of construct height and a shear amplitude of 0.4 mm. Our previous experiments suggested that mRNA levels peaked at 2 h post-completion of mechanical loading [34]. Therefore, quantitative real-time polymerase chain reaction (qRT-PCR) was conducted 2 h after loading had ceased.

Constructs were homogenized in 1 ml of TRIzol reagent (Invitrogen), and total RNA was isolated according to the manufacturer's instructions (n=6). A SuperScript™ III First Strand Synthesis System (Invitrogen) was used to synthesize complementary DNA (cDNA). DNase and RNase digestions were performed before and after cDNA synthesis, respectively. qRT-PCR was carried out using SybrGreen® Mastermix (Invitrogen) and a QuantStudio™ 7 Flex Real-Time PCR system (Applied Biosystems). The cycle threshold (C_t) value of each gene was normalized to the geometric mean of the housekeeping genes *RPL13A* using the comparative C_t method ($2^{-\Delta Ct}$). Primer sequences were used as published previously (*COL1A1* [36], *COL2A1* [36], *ACAN* [36], *PRG4* [36], *RPL13A* [37]).

2.9 Statistical analysis

All quantitative data were evaluated with GraphPad v6.05 (GraphPad Software, Inc., USA) and expressed as means ± SD. Statistical significance was determined using Student's t-test or one-way ANOVA followed by Tukey Kramer test for pair-wise comparisons, where appropriate, with $p<0.05$ considered significant

3 Results and discussion

3.1 Morphology of fibrous networks, hydrogels and fiber-reinforced hydrogels

Representative FE-SEM micrographs of the network architectures printed via MEW at 200, 400 and 600 µm fiber spacing and 0° - 90° lay-down pattern are shown in Figure 1b-d. Irrespective of fibrous network type, the fibers exhibited continuity and a consistent average fiber diameter of 21.36 ± 1.37 µm along each construct. This fibre diameter provides higher surface area to volume ratio in comparison to conventional melt-extrusion based additive manufacturing techniques such as fused deposition modelling [38] and bioextrusion [39], where filament diameters of >~250 µm are often reported. Although the accuracy of the fiber positioning decreased when the fiber spacing was reduced, the intended 0°-90° crosshatch architecture was highly coherent for all the fibrous networks. For the fibrous networks with a 600-µm fiber spacing, fibers were deposited with high accuracy on top of each other along the entire thickness, whereas for the fibrous networks with a 200- and 400-µm fiber spacing, a small number of fibers were also found in between the pores. Gross morphology characterization of the resulting fiber-reinforced hydrogels by via both stereomicroscopy and MRI demonstrated the high infiltration degree of the gels into the pores of the fibrous networks, and only few small air bubbles entrapped within constructs were identified (Figures 1f and g).

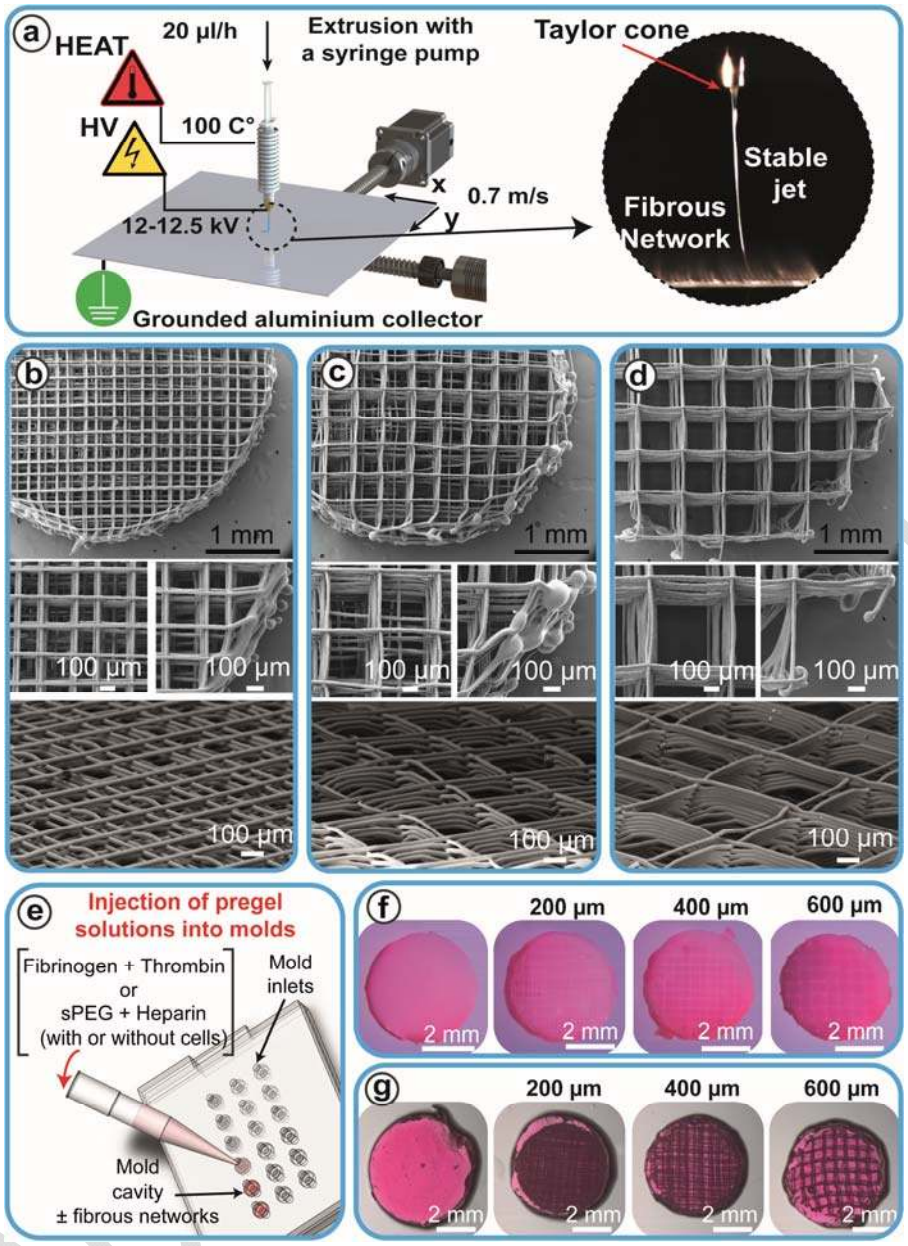

Figure 1. (a) Graphical representation of a MEW device showing the optimized printing parameters used to manufacture reinforcing fibrous networks for this study. These parameters yield a sustainable Taylor cone formation and a stable polymeric jet, as shown. MEW enabled a good control over the deposition of the fibers, where the intended 0°-90° crosshatch architecture and the 200-µm (b), 400-µm (c), and 600-µm (d) fiber spacing of the printed fibrous networks were highly regular and coherent. Fibers exhibit a good continuity with a consistent average diameter of 21.36 ± 1.37 µm along each construct. Magnified insets highlighting the pore size and laser cut edges of the fibrous networks show a custom-made injection molding system used for the preparation of fiber-reinforced hydrogels (e), and stereomicroscopy images of fibrin (f) and sPEG/Hep (g) hydrogels, with and without reinforcing fibrous networks.

3.2 Mechanical properties of hydrogels, fibrous networks, fiber-reinforced hydrogels and biomimetic reinforcement mechanism of soft network composites

The majority of fiber-reinforced samples, especially sPEG/Hep matrix composites, displayed a pronounced *J*-shaped stress/strain (σ/ε) curve during unconfined compression (Figure 2a). This distinctive behavior, characterized by a gradual increase of the tangent modulus with increasing extension, is particularly common in natural fiber-reinforced soft matrix tissues, including articular cartilage [40,41]. In natural materials, this mechanical response is mostly attributed to the uncoiling and straightening of the collagen fibrils at low displacement rates inside a soft matrix until the fibrils start bearing the load [40]. An analogous behavior was observed at a macroscopic level when compressing the fiber-reinforced hydrogels (Video S1). Importantly, the range of the recorded stress values reached those of articular cartilage. Composite samples first exhibited a very low and flat stress profile at a compressive strain of approximately < 2.5% (toe region), which started to increase substantially with increasing compressive strain (heel region; approximately between 2.5 – 10% strain). At the heel region, slightly sagged/kinked fibers aligned and stretched, leading to a sharp upward transition on the σ/ε curve. Finally, once the fibers of the composites became taut, σ/ε profiles displayed a linear trend, similar to the native cartilage behavior. It is important to emphasize that some hydrogels also displayed a nonlinearity, likely due to the alignment and tensioning of their polymer chains [42–44]. Although the video capturing the deformation of a fiber-reinforced hydrogel and the high range of the resulting stress values strongly suggest that the nonlinearity of fiber-reinforced hydrogels was primarily originating from the reformation of the fibers, hydrogels may also, to some extent, have contributed to the nonlinear behavior at a molecular level.

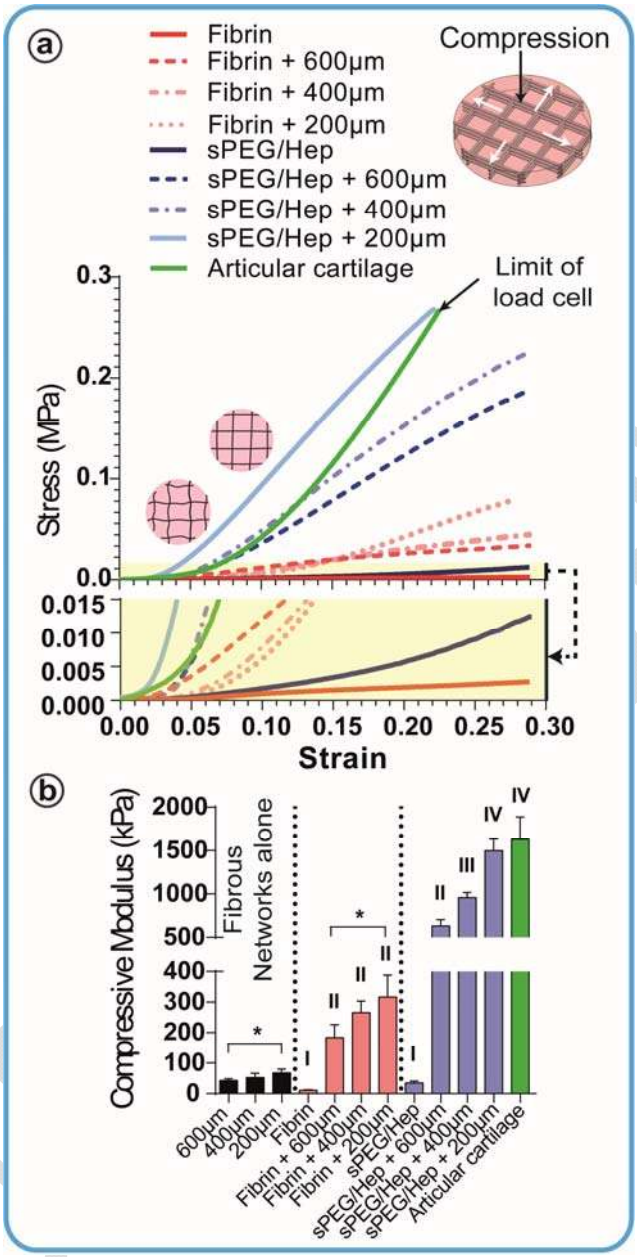

Figure 2. Mechanical properties of hydrogels, fibrous networks, fiber-reinforced hydrogels and biomimetic reinforcement mechanism of soft network composites: (a) Representative stress-strain graphs of hydrogels and fiber-reinforced hydrogels in comparison to articular cartilage exhibiting *J*-shaped curve. Fiber alignment and stretching at the different stages of compression were schematically illustrated; and (b) Unconfined compressive moduli (E) of fibrous networks, hydrogels, fiber-reinforced hydrogels and articular cartilage. Different Roman numerals and the asterisk indicate a significant difference between each group ($n = 6$, $p < 0.05$).

Compressive moduli (E) of fibrin (E_{Fibrin}) and sPEG/Hep ($E_{sPEG/Hep}$) alone were 10.6 ± 2.5 and 35.0 ± 5.9 kPa, respectively (Figure 2b). Similarly, E of the fibrous networks alone was

considerably low in comparison to that of human articular cartilage ($E_{\text{Network 600μm}}$ = 43.0 ± 6.2 kPa; $E_{\text{Network 400μm}}$ = 52.8 ± 13.7 kPa; $E_{\text{Network 200μm}}$ = 67.5 ± 12.3 kPa, and $E_{\text{Cartilage}}$ = 1629.0 ± 256.5 kPa) (n=6). Remarkably, E of the fiber-reinforced hydrogels was up to 29-fold and 42-fold higher than E_{Fibrin} and $E_{\text{sPEG/Hep}}$, respectively, and up to 4-fold and 14-fold higher than E_{Fibrin}+ E_{Network} and $E_{\text{PEG/Hep}}$+ E_{Network}, respectively, suggesting that reinforcement is occurring through a synergistic interaction between the fibrous network and hydrogel constituents. According to our observations and previous findings [16,17], fibrous networks alone fail under compressive loads due to buckling, fiber delamination and misalignment or skewing of the entire construct and therefore, they possess only limited compressive mechanical strength. This is in line with the fact that fibers are often stronger in tension in comparison to compression. Also, due to their poor mechanical properties, hydrogels lose integrity and undergo mechanical failure at low magnitudes of forces. However, the incorporation of fibrous networks within the hydrogels overcomes the limitations of both constituents of the system (Figure 2b). In the composites, the hydrogels expand laterally between the pores of the fibrous networks under compressive loads, thus stretching the fibers. This allows fibers to carry the compressive loads applied to the composites in tensile form. Simultaneously, the integrity of the soft hydrogel matrix is maintained due to the confinement of high-modulus fibers. Inclusion of different fibrous networks in hydrogels led to different degrees of mechanical reinforcements (Table S1). $E_{\text{Composite}}$ increased with decreasing fiber spacing, likely because of the higher reinforcing filler ratio. It should be noted that the scope of the study was not only to design composites with biomimetic mechanical properties, but also to utilize the attractive biological properties of soft hydrogels. In this regard, hydrogels were retained as the primary constituent of the composites where the volumetric hydrogel fraction of the fiber-reinforced samples was 88.4 ± 0.3%, 91.9 ± 0.2 % and 94.4 ± 0.3 % for the constructs reinforced with 200-μm, 400-μm, and 600-μm pore-sized fibrous networks, respectively (n=30).

To compare the time-dependent mechanical properties of the fibrous networks, hydrogels and soft network composites with articular cartilage, we performed step-wise stress-relaxation tests consisting of 4 steps of 5% compressive strain ramps, each followed by an equilibrium period in an unconfined compression (n=4). As seen in the stress vs. time (σ/t) profiles (Figure 3a), fibrous networks did not show a high degree of relaxation over time. It has been shown that substrates exhibiting a high degree of stress relaxation upon loading enhance the spreading, proliferation and regulate the fate of mesenchymal stem cells, suggesting that stress-relaxation is a fundamental criterion of biomaterials design when culturing mechanosensitive cells [45]. Similarly to fibrous networks alone, such relaxation behavior was not present in sPEG/Hep hydrogels (Figure 3c). In contrast, the stress decay of fibrin was very sharp and deep after each compression ramp, and equilibrium was reached with rapid relaxation (Figure 3b). Nevertheless, none of the hydrogels and fibrous networks alone displayed an σ/t profile comparable to that of articular cartilage, and the resulting equilibrium moduli ($E_{Eq.}$) values were considerably lower (Figure 3d). Although the relaxation of articular cartilage was slightly slower, Figures 3b-c show that the mechanical response of fiber-reinforced hydrogels to a stepwise stress-relaxation test resembles that of the native tissue. Specifically, sPEG/Hep + 200-μm fibrous network samples displayed similarity to articular cartilage both mechanistically and magnitude-wise (for numerical comparison, see Table 1).

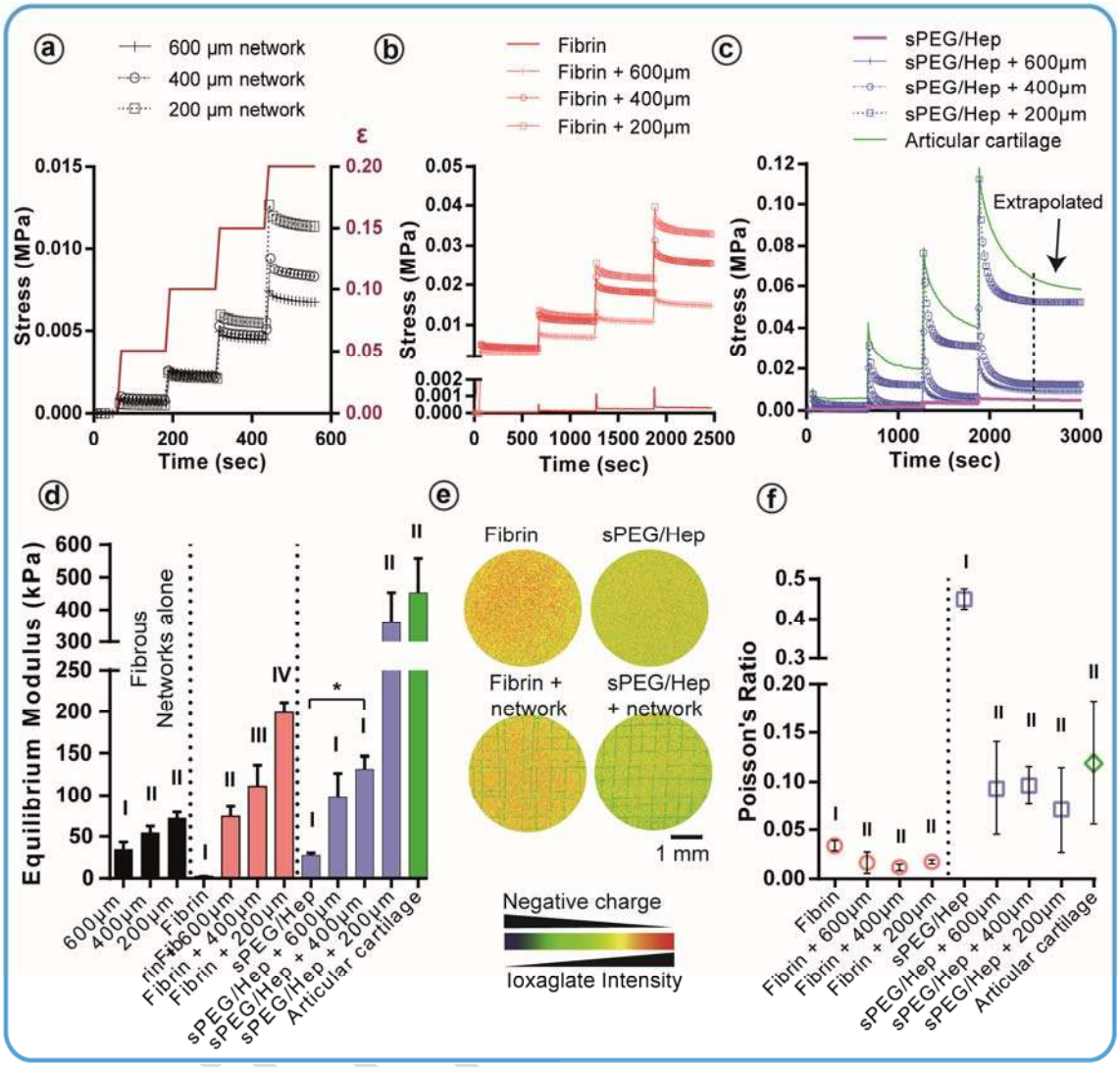

Figure 3. (a-c): Typical stress-behavior of fibrous networks (a), fibrin and fiber-reinforced fibrin (b), sPEG/Hep, fiber-reinforced sPEG/Hep and articular cartilage (c), in response to ramp displacements. (d): Unconfined equilibrium moduli ($E_{Eq.}$) of hydrogels, fibrous networks, fiber-reinforced hydrogels and articular cartilage. (e): Epic-µCT scans of cell-free fibrin and sPEG/Hep with reinforced counterparts illustrating the differences in the negative charge density. (f): Poisson's ratio (ν) of hydrogels, fibrous networks, fiber-reinforced hydrogels and articular cartilage.

Figure 3c depicts that once articular cartilage is exposed to external mechanical stimuli, it exhibits a high compressive stress that diminishes gradually over time. This can be explained by the complex dynamic interplays between the interstitial fluid and the solid constituents of the tissue [46–48]. Previous studies suggested that the exudation of the interstitial fluids does not occur rapidly. and therefore, compressive loads applied at high strain rates promote the

pressurization of these fluids restrained by the crosslinked solid constituents of the tissue [49,50]. Also, this pressurization induces the collagen fibrils of the tissue, which are considered to have low resistance in compression compared to their ability to carry tensile loads, to undertake the loads in tensile form [48,51,52]. Thus, articular cartilage exhibits high stress peaks when loaded at high strain rates [53,54]. Conversely, the transient response of the tissue is more similar to that of the equilibrium when it is subjected to displacements at low strain rates [55]. After each stress peak, eventual relaxation occurs gradually through the reorganization of the solid matrix constituents and the redistribution or loss of the interstitial fluid [56].

Since kinetics and outflow of interstitial fluid govern the strain- and time-dependent mechanical properties of the tissue, we investigated the behavior of water in our hydrogels under compressive loading. We first compressed the hydrogel-only samples to 20% strain and measured the water loss upon loading gravimetrically. Similarly to hydrated soft tissues, hydrogels are known to undergo both volumetric and gravimetric changes through water loss in response to a compressive loading [57]. We also observed weight reductions of $22.0 \pm 6.6\%$ and $1.9 \pm 0.6\%$ in compressed fibrin and sPEG/Hep hydrogels, respectively. Results are in accordance with the fact that heparin is a highly negatively charged glycosaminoglycan (GAG), and thus, it strongly attracts water through dipole-dipole interactions [58]. Hence, water molecules absorbed by sPEG/Hep hydrogels may have a reduced degree of freedom and therefore. compression-induced water outflow from the hydrogel matrix would be hindered. To test this hypothesis, we compared the fixed negative charge density of the samples by equilibrium partitioning of an ionic contrast agent-microcomputed tomography (EPIC-μCT) [59] using ioxaglate, a negatively charged contrast agent. Results showed that the intensity of the signal from the contrast agent, depicted in red coloring, was weaker in sPEG/Hep-based constructs compared to fibrin-based samples, likely because of the stronger repulsion of the

agent (Figure 3e and Figure S4). This confirmed that sPEG/Hep has a higher fixed negative charge density than fibrin, indicating that water binds more strongly to the sPEG/Hep. Furthermore, Poisson's ratio (v), a material property which is defined as the negative ratio of transverse to longitudinal strain, of the constructs was measured during the stepwise stress-relaxation tests (Figure 3f). Results showed that v_{Fibrin} was 0.03 ± 0.01, indicating that compressed fibrin undergoes a significant volumetric loss, whereas $v_{sPEG/Hep}$ was 0.45 ± 0.03, which indicates a good volumetric conservation in long-term loading. Since hydrogels are primarily made of water, an almost perfectly incompressible material, they are very likely to exhibit a high initial v when loaded at high strain rates. Therefore, both types of hydrogels give rise simultaneously to matrix pressurization and fiber-tensioning mechanisms similar to those observed in native articular cartilage at rapid loading. This was reflected on the σ/t curves of fiber-reinforced composites as high stress peaks. However, owing to its high water retention capacity, sPEG/Hep expands laterally with an initial v value close to 0.5 and maintains a good volumetric stability as measured by $v_{sPEG/Hep}$ (0.45 ± 0.03) under prolonged loading conditions. Thus, stress peaks were more pronounced in sPEG/Hep- than fibrin-based fiber-reinforced composites. Also, the resulting equilibrium moduli of reinforced sPEG/Hep hydrogels were higher than E_{Eq} of the reinforced fibrin hydrogels and reached that of articular cartilage. Similarly to articular cartilage, flow kinetics of interstitial water controls the matrix pressurization/relaxation levels within the fiber-reinforced hydrogels and therefore plays a key role in the transient and equilibrium mechanical behavior. As reviewed by Ateshian, both experimental findings and theoretical models suggest that pressurization of the interstitial fluid of ECM is the primary regulator of the excellent lubrication mechanism of articular cartilage [60]. The friction coefficient of the tissue is at its lowest when the load is primarily carried by the pressurized fluid. We hypothesize that fiber-reinforced hydrogels might express a similar self-lubricating behavior due to the observed hydrogel and fluid pressurization in response to

compressive loading. Lastly, Poisson's ratio of the reinforced hydrogels was significantly lower than that of their hydrogels only counterparts, suggesting that the lateral expansion of the reinforced hydrogels is partially constrained by the fibers (Figure 3f). It was suggested that, due to the compaction of the solid constituents of the tissue, the permeability of articular cartilage decreases as the compressive strain increases [61]. The reduction in the radially directed permeability was shown to be significantly higher than the axially directed permeability [62]. In reinforced hydrogels, while the polymeric network of the hydrogel matrix becomes denser with increasing compression, the size of lateral pores between the fibers is also gradually decreasing. Considering that fibers do not allow fluids to pass through them, we expect that fiber-reinforced hydrogels may show a similar anisotropic strain-dependent permeability.

Soft matrix tissues, including articular cartilage, exhibit viscoelasticity [56]. Despite being one of the essential characteristics of natural materials, viscoelasticity is often overlooked in the design and characterization of biomaterials [63]. It is also known that alteration of substrate viscoelasticity has a direct influence on the behavior of seeded cell populations [64,65]. To investigate the viscoelasticity of our constructs, we performed dynamic mechanical analysis by applying one hundred cycles of a sinusoidal compressive strain at an amplitude of 2.5% and frequency of 0.1 Hz (Figure 4a-c). As expected, fibrous networks alone exhibited a considerably low loss factor (loss modulus (E'')/storage modulus(E')), a parameter defined as the ratio of viscous liquid-like behavior to elastic solid-like behavior. This is an indication of prominent elasticity. sPEG/Hep was also found to be highly elastic. Conversely, fibrin displayed a considerably high loss factor, indicating high energy dissipation efficiency. However, fibrin's low loss modulus value significantly restricts its capacity to damp high applied loads. Fiber reinforcement had different effects on E''/E' with respect to the hydrogel type, either increased or decreased, but E''/E' of the resulting composites were closer to that of articular cartilage. Both E' and E'' of the composites were significantly higher than those of their hydrogel alone

and fibrous network alone counterparts, and closer to that of articular cartilage (Figure 4b-c). Specifically, sPEG/Hep hydrogels reinforced with a 200 µm fibrous network displayed a viscoelasticity similar to that of articular cartilage, characterized by *E′, E″ and E″/E′*. This may represent a significant advantage for applications that require high energy dissipations such as high load-bearing tissue substitutes.

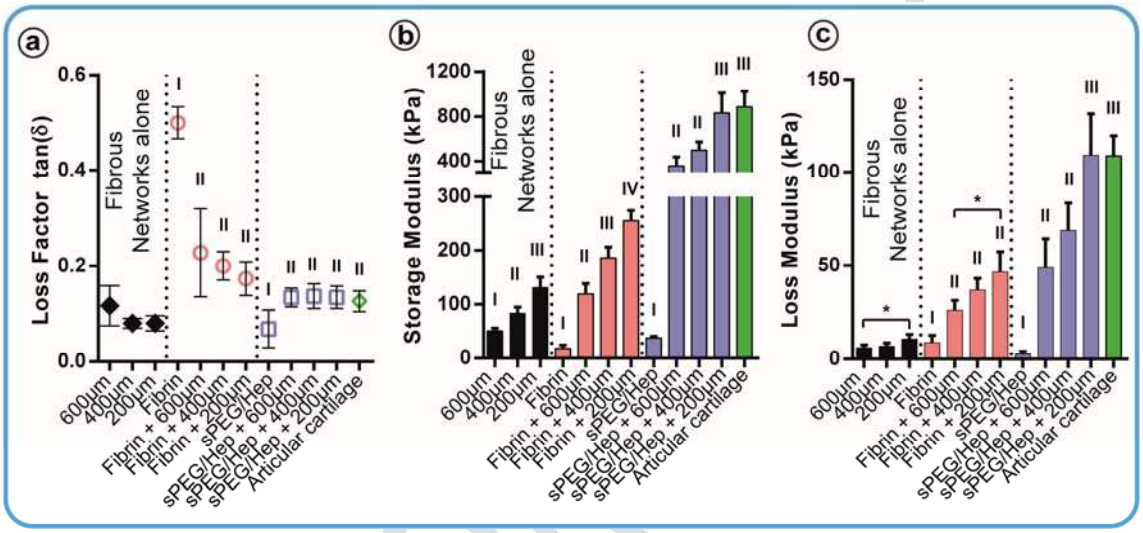

Figure 4. Dynamic mechanical properties of the fibrous networks, hydrogels, fiber-reinforced hydrogels and articular cartilage, including: (a) Loss factor (*E″/E′*), (b) Storage (*E′*), and (c) Loss (*E″*) moduli. Different Roman numerals and the asterisk indicate a significant difference within each group (in the mechanical tests; n = 4 and $p < 0.05$).

Table 1. Basic biomechanical properties of hydrogels and selected fiber-reinforced hydrogels compared to native articular cartilage. *Poisson's ratio (ν) of the samples was measured in step-wise stress relaxation tests.

	Compressive Modulus (E) (kPa)	Equilibrium Modulus ($E_{Eq.}$) (kPa)	Equilibrium Poisson's Ratio (ν)*	Loss Factor (tanδ)
Fibrin	10.61 ± 2.51	2.27 ± 0.29	0.03 ± 0.01	0.50 ± 0.03
sPEG/Hep	34.99 ± 5.87	27.80 ± 3.09	0.45 ± 0.03	0.07 ± 0.04
Fibrin + 200µm network	316.73 ± 71.34	199.00 ± 11.86	0.02 ± 0.01	0.18 ± 0.03

sPEG/Hep + 200μm network	1497.05 ± 138.26	370.97 ± 88.94	0.07 ± 0.04	0.13 ± 0.02
Human articular cartilage (experiments)	1629.30 ± 256.48	452 ± 104	0.12 ± 0.06	0.12 ± 0.02
Human articular cartilage literature)	~1750-2250 [63]	~200-400 [63], ~200-580 [66] ~250-500 [67]	~0-0.1 [68–70], 0.16 [66], 0.26 [54] ~0.15-0.25 [67]	~0.16-0.17 [63]

3.3 Simulations

To further advance our insights into the reinforcement mechanism at rapid loading, a numerical model was developed using the p-version of the FEM (p-FEM). The basic discretization principle of p-FEM is based on keeping the computational mesh fixed and improving the accuracy by increasing the polynomial degree of each mesh-element [71]. This is in contrast to the classical approach available in commercial software, where the size of the elements composing the mesh is decreased to obtain higher accuracy (h-FEM). High-order FEM has been shown to provide more accurate results in elements with high aspect ratio at a lower cost compared to h-FEM [32]. Because of the idealization of the geometry and the absence of plasticity in the simulations, the fibrous networks alone exhibited a higher stiffness in silico compared to experimental samples. Simulated and experimental data were otherwise in good agreement both qualitatively and quantitatively (Figure 5a-d) (Video S2). In fibrous network alone samples, the load was primarily carried by the fiber junctions whereas the fibers in the reinforced model were also carrying tensional load because of the expanding gel. Simulations also revealed that fiber-reinforced hydrogels have a mechanical anisotropy. E of fiber-reinforced hydrogels was highly dependent on the loading direction (from top or side), in contrast to bulk hydrogels.

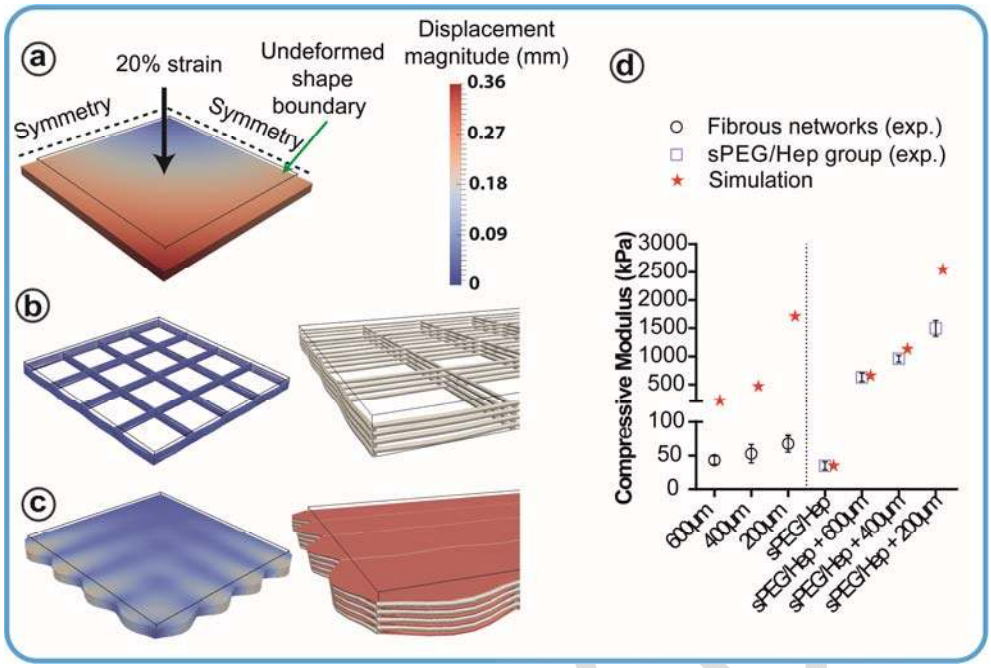

Figure 5. Simulated displacement behavior and deformed configurations of: (a) sPEG/Hep alone, (b) 600 μm fibrous network, and (c) sPEG/Hep + 600 μm fibrous network composite for a given compression level (20% strain). Compressive moduli values (d) were determined from the simulations in comparison to the experimental data. (EPEG/Hep and EPCL values measured in the experiments were used to model the hydrogel and fibers in silico, respectively. νGEL was taken as 0.495 assuming that the hydrogel phase is nearly incompressible at rapid loading and ν_{mPCL} was taken as 0.3).

In addition to the experimentally identified quantitative and behavioral similarities between the soft composite networks and the native articular cartilage, a morphological analogy could also be drawn. Indeed, collagen fibrils of articular cartilage are mimicked by microfibers, and interstitial water and proteoglycans are presented by the water-saturated hydrogel matrix. In the case of sPEG/Hep hydrogels, signs of charge-driven-osmosis were identified. This phenomenon is also present in articular cartilage and is speculated to stem from the negative charges of proteoglycans [56]. In this regard, with a high negative charge density and a strong water retention capacity, heparin crosslinked with PEG brings another dimension to the biomimetic concept through the mechano-electrochemical emulation of the tissue.

3.4 Cell viability and cellular response to physiologically relevant loading

In vitro studies were carried out to demonstrate the capacity of fiber-reinforced hydrogels to provide a suitable microenvironment for chondrocyte culture and neocartilage formation. In order to benefit from the superior biological properties of the hydrogel [20,35], we chose composites reinforced with 600μm pore-sized fibrous networks for our preliminary *in vitro* study, which presented the highest volumetric hydrogel fraction among our samples. Human chondrocytes were encapsulated in sPEG/Hep hydrogels with and without fiber-reinforcement and cultured under static conditions for 14 days before a 1 h unconfined biaxial mechanical stimulation to investigate cellular response to physiologically relevant loading. A high cell viability (> 80%) was observed in hydrogels with and without reinforcement, at both days 1 and 14 (Figure 6a-c). Short-term compressive/shear stimulation led to an up-regulation of the chondrogenic marker genes *ACAN* and *COL2A1*, as well as the de-differentiation marker *COL1A1* in sPEG/HEP hydrogels without fiber reinforcement (Figure 6d-e). The transcriptional response of chondrocytes encapsulated in fiber-reinforced sPEG/HEP to loading was, however, less distinctive, suggesting that dynamic culture parameters such as the applied strain level, loading frequency, and loading duration may require further optimization to induce statistically significant anabolic responses similar to sPEG/HEP alone. Interestingly, the expression levels of *ACAN*, *COL2A1*, and the superficial chondrocyte marker *PRG4* were generally higher than in sPEG/HEP alone while *COL1A1* expression was similar, suggesting improved chondrogenic differentiation of the cells encapsulated in fiber-reinforced constructs (**Figure 6e**). While we have not investigated the underlying mechanisms in the present study, it is likely that chondrogenesis was promoted by increased hydrostatic pressure (HP) within fiber-reinforced constructs compared to sPEG/HEP alone. It is well established that HP promotes proteoglycan and collagen type II mRNA and protein expression of chondrocytes cultured on monolayer, scaffolds, or in scaffold-less 3D constructs, leading to tissue-engineered cartilage constructs

with improved physicochemical properties [72]. Similar to the predominant mechanism governing the compressive properties of native cartilage, fixed negative charges facilitated by co-polymerised heparin in our system attract water which leads to hydrogel swelling. While non-reinforced gels can swell freely until equilibrium is reached, fiber-reinforcement restricts hydrogel swelling analogous to the collagen network in articular cartilage which, in turn, leads to enhanced compressive strength and chondrogenesis facilitated by HP.

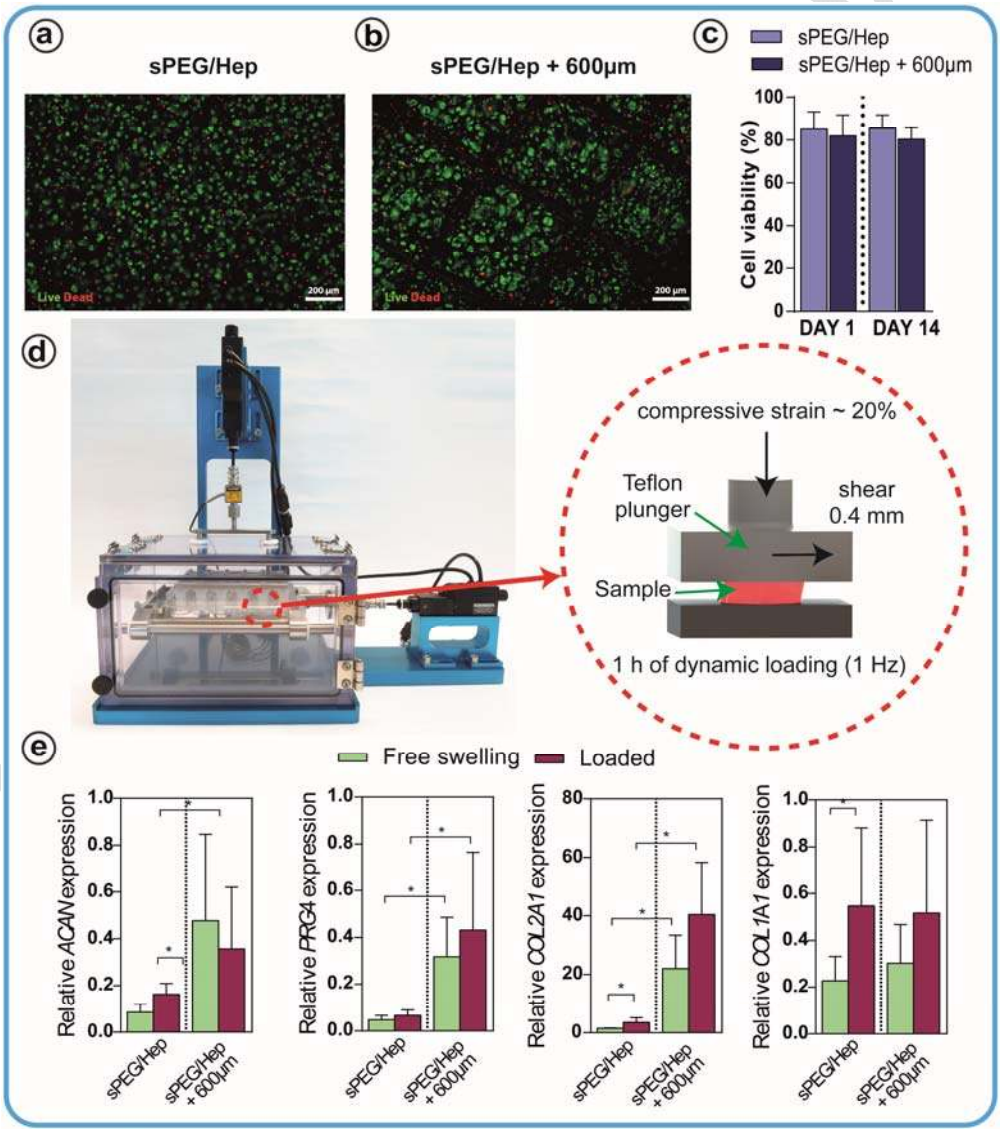

Figure 6. Viability of the encapsulated human chondrocytes in: (a) sPEG/Hep, and (b) fiber-reinforced sPEG/Hep at day 14. c) Quantification of the viable and dead cells. d) Photo of the biaxial loading bioreactor and the schematic representation of a gel being mechanically stimulated with the loading protocol used. e) Gene expression levels of encapsulated cells under

free swelling and loaded conditions (data were normalized to the housekeeping gene *RPL13A*). The asterisk indicates a significant difference ($p < 0.05$).

4 Conclusion

To our knowledge, this study is the first to present biofabricated fiber-reinforced hydrogels that capture the overall transient, equilibrium and dynamic mechanical behavior of articular cartilage. sPEG/Hep hydrogels were reinforced using highly-ordered melt electrospun network architectures to mimic the wide-ranging biomechanical performance of articular cartilage. These soft network composites were found to be viscoelastic, mechanically nonlinear and anisotropic. The constructs also exhibited enhanced biological performance, as depicted by high chondrocyte viability and differentiation under physiologically relevant loading. Moreover, because of the high negative charge density and strong water retention capacity of the heparin-crosslinked with PEG leading to a charge-driven osmosis, a mechano-electrochemical emulation of the cartilage tissue was achieved. Finally, computational simulations were in line with the experimental findings. Together, our data suggest that the bioinspired soft matrix fiber-reinforcing concept used in this study in combination with computational models could not only be employed for cartilage tissue engineering, but may also allow for the deterministic design of biomechanically robust composites for other tissue engineering applications such as skin, heart valve or breast.

Acknowledgements

DWH would like to acknowledge support from the Australian Research Council under the ARC Training Centre in Additive Biomanufacturing, National Health and Medical Research Council and IAS-TUM (Hans Fischer Senior Fellowship). TK would like to acknowledge support from the ARC through his Future Fellowship (FT110100166) and the ARC Training Centre in Additive Biomanufacturing. DD would like to acknowledge Technische Universität München-

Institute for Advanced Study, funded by the German Excellence Initiative and the European Union Seventh Framework Programme under grant agreement n. 291763.

References

[1] Saito T, Oaki Y, Nishimura T, Isogai A and Kato T 2014 Bioinspired stiff and flexible composites of nanocellulose-reinforced amorphous CaCO3 *Mater. Horizons* **1** 321

[2] Wegst U G K, Bai H, Saiz E, Tomsia A P and Ritchie R O 2015 Bioinspired structural materials *Nat Mater* **14** 23–36

[3] Jang K-I, Chung H U, Xu S, Lee C H, Luan H, Jeong J, Cheng H, Kim G-T, Han S Y, Lee J W, Kim J, Cho M, Miao F, Yang Y, Jung H N, Flavin M, Liu H, Kong G W, Yu K J, Rhee S Il, Chung J, Kim B, Kwak J W, Yun M H, Kim J Y, Song Y M, Paik U, Zhang Y, Huang Y and Rogers J A 2015 Soft network composite materials with deterministic and bio-inspired designs *Nat. Commun.* **6** 6566

[4] Xu H, Xie L, Chen J-B, Jiang X, Hsiao B S, Zhong G-J, Fu Q and Li Z-M 2014 Strong and tough micro/nanostructured poly(lactic acid) by mimicking the multifunctional hierarchy of shell *Mater. Horizons* **1** 546

[5] Mayer G 2005 Rigid biological systems as models for synthetic composites. *Science* **310** 1144–7

[6] Podsiadlo P, Kaushik A K, Arruda E M, Waas A M, Shim B S, Xu J, Nandivada H, Pumplin B G, Lahann J, Ramamoorthy A and Kotov N A 2007 Ultrastrong and stiff layered polymer nanocomposites. *Science* **318** 80–3

[7] Munch E, Launey M E, Alsem D H, Saiz E, Tomsia A P and Ritchie R O 2008 Tough, Bio-Inspired Hybrid Materials *Science (80-.).* **322** 1516–20

[8] Palmqvist A E C 2003 Synthesis of ordered mesoporous materials using surfactant liquid crystals or micellar solutions *Curr. Opin. Colloid Interface Sci.* **8** 145–55

[9] Dunlop J W C and Fratzl P 2010 Biological Composites *Annu. Rev. Mater. Res.* **40** 1–24

[10] Aspden R M 1994 Fibre reinforcing by collagen in cartilage and soft connective tissues. *Proc. Biol. Sci.* **258** 195–200

[11] Moutos F T, Freed L E and Guilak F 2007 A biomimetic three-dimensional woven composite scaffold for functional tissue engineering of cartilage. *Nat. Mater.* **6** 162–7

[12] Van Lieshout M, Peters G, Rutten M and Baaijens F 2006 A knitted, fibrin-covered polycaprolactone scaffold for tissue engineering of the aortic valve. *Tissue Eng.* **12** 481–7

[13] Eslami M, Vrana N E, Zorlutuna P, Sant S, Jung S, Masoumi N, Khavari-Nejad R A, Javadi G and Khademhosseini A 2014 Fiber-reinforced hydrogel scaffolds for heart valve tissue engineering. *J. Biomater. Appl.* **29**0885328214530589-

[14] Strange D G T, Tonsomboon K and Oyen M L 2014 Mechanical behaviour of electrospun fibre-reinforced hydrogels *J. Mater. Sci. Mater. Med.* **25** 681–90

[15] Marijnissen W J C M, Van Osch G J V M, Aigner J, Van Der Veen S W, Hollander A P, Verwoerd-Verhoef H L and Verhaar J A N 2002 Alginate as a chondrocyte-delivery substance in combination with a non-woven scaffold for cartilage tissue engineering *Biomaterials* **23** 1511–7

[16] Bas O, De-Juan-Pardo E M, Chhaya M P, Wunner F M, Jeon J E, Klein T J and Hutmacher D W 2015 Enhancing structural integrity of hydrogels by using highly organised melt electrospun fibre constructs *Eur. Polym. J.* **72** 451–63

[17] Visser J, Melchels F P W, Jeon J E, van Bussel E M, Kimpton L S, Byrne H M, Dhert W J A, Dalton P D, Hutmacher D W and Malda J 2015 Reinforcement of hydrogels using three-dimensionally printed microfibres. *Nat. Commun.* **6** 6933

[18] Tsurkan M V., Chwalek K, Prokoph S, Zieris A, Levental K R, Freudenberg U and Werner C 2013 Defined polymer-peptide conjugates to form cell-instructive starpeg-heparin matrices in situ *Adv. Mater.* **25** 2606–10

[19] Kim M, Shin Y, Hong B-H, Kim Y-J, Chun J-S, Tae G and Kim Y H 2010 In vitro chondrocyte culture in a heparin-based hydrogel for cartilage regeneration. *Tissue Eng. Part C. Methods* **16** 1–10

[20] Zieris A, Prokoph S, Levental K R, Welzel P B, Grimmer M, Freudenberg U and Werner C 2010 FGF-2 and VEGF functionalization of starPEG–heparin hydrogels to modulate biomolecular and physical cues of angiogenesis *Biomaterials* **31** 7985–94

[21] Freudenberg U, Hermann A, Welzel P B, Stirl K, Schwarz S C, Grimmer M, Zieris A, Panyanuwat W, Zschoche S, Meinhold D, Storch A and Werner C 2009 A star-PEG–heparin hydrogel platform to aid cell replacement therapies for neurodegenerative diseases *Biomaterials* **30** 5049–60

[22] Liang Y and Kiick K L 2014 Heparin-functionalized polymeric biomaterials in tissue engineering and drug delivery applications *Acta Biomater.* **10** 1588–600

[23] Baldwin J G, Wagner F, Martine L C, Holzapfel B M, Theodoropoulos C, Bas O, Savi F M, Werner C, De-Juan-Pardo E M and Hutmacher D W 2017 Periosteum tissue engineering in an orthotopic in vivo platform *Biomaterials* **121** 193–204

[24] Catelas I 2011 Fibrin *Compr. Biomater.* **2** 303–28

[25] Eyrich D, Brandl F, Appel B, Wiese H, Maier G, Wenzel M, Staudenmaier R, Goepferich A and Blunk T 2007 Long-term stable fibrin gels for cartilage engineering *Biomaterials* **28** 55–65

[26] Passaretti D, Silverman R P, Huang W, Kirchhoff C H, Ashiku S, Randolph M A and Yaremchuk M J 2001 Cultured chondrocytes produce injectable tissue-engineered cartilage in hydrogel polymer. *Tissue Eng.* **7** 805–15

[27] Brown T D, Dalton P D and Hutmacher D W 2011 Direct Writing By Way of Melt Electrospinning *Adv. Mater.* **23** 5651–7

[28] Vaquette C, Ivanovski S, Hamlet S M and Hutmacher D W 2013 Effect of culture

conditions and calcium phosphate coating on ectopic bone formation. *Biomaterials* **34** 5538–51

[29] Meyers M A and Chawla K K 2009 Mechanical Behavior of Materials *Cambridge, Cambridge Univ. Press* 121–5

[30] Tan E P S, Ng S Y and Lim C T 2005 Tensile testing of a single ultrafine polymeric fiber. *Biomaterials* **26** 1453–6

[31] Levett P, Melchels F P W, Schrobback K, Hutmacher D W, Malda J and Klein T J 2014 A biomimetic extracellular matrix for cartilage tissue engineering centered on photocurable gelatin, hyaluronic acid and chondroitin sulfate. *Acta Biomater.* **10** 214–23

[32] Rank E, Düster A, Nübel V, Preusch K and Bruhns O T 2005 High order finite elements for shells *Comput. Methods Appl. Mech. Eng.* **194** 2494–512

[33] Szabó B and Babuška I 2011 Generalized Formulations *Introduction to Finite Element Analysis* (John Wiley & Sons, Ltd) pp 109–44

[34] Jeon J E, Schrobback K, Meinert C, Sramek V, Hutmacher D W and Klein T J 2013 Effect of preculture and loading on expression of matrix molecules, matrix metalloproteinases, and cytokines by expanded osteoarthritic chondrocytes *Arthritis Rheum.* **65** 2356–67

[35] Slaughter B V, Khurshid S S, Fisher O Z, Khademhosseini A and Peppas N a 2009 Hydrogels in regenerative medicine. *Adv. Mater.* **21** 3307–29

[36] Schrobback K, Malda J, Crawford R W, Upton Z, Leavesley D I and Klein T J 2012 Effects of Oxygen on Zonal Marker Expression in Human Articular Chondrocytes *Tissue Eng. Part A* **0** 1–14

[37] Schrobback K, Wrobel J, Hutmacher D W, Woodfield T B F and Klein T J 2013 Stage-specific embryonic antigen-4 is not a marker for chondrogenic and osteogenic potential in cultured chondrocytes and mesenchymal progenitor cells. *Tissue Eng. Part A* **19** 1316–26

[38] Zein I, Hutmacher D W, Tan K C and Teoh S H 2002 Fused deposition modeling of novel scaffold architectures for tissue engineering applications. *Biomaterials* **23** 1169–85

[39] Domingos M, Dinucci D, Cometa S, Alderighi M, Bártolo P J and Chiellini F 2009 Polycaprolactone Scaffolds Fabricated via Bioextrusion for Tissue Engineering Applications. *Int. J. Biomater.* **2009** 239643

[40] Chen P-Y, McKittrick J and Meyers M A 2012 Biological materials: Functional adaptations and bioinspired designs *Prog. Mater. Sci.* **57** 1492–704

[41] Sacks M S and Yoganathan A P 2007 Heart valve function: a biomechanical perspective. *Philos. Trans. R. Soc. Lond. B. Biol. Sci.* **362** 1369–91

[42] Drury J L, Dennis R G and Mooney D J 2004 The tensile properties of alginate hydrogels *Biomaterials* **25** 3187–99

[43] Lee S-Y, Pereira B P, Yusof N, Selvaratnam L, Yu Z, Abbas A A and Kamarul T 2009

Unconfined compression properties of a porous poly(vinyl alcohol)-chitosan-based hydrogel after hydration. *Acta Biomater.* **5** 1919–25

[44] Hashemnejad S M and Kundu S 2016 Strain stiffening and negative normal stress in alginate hydrogels *J. Polym. Sci. Part B Polym. Phys.* 1–9

[45] Chaudhuri O, Gu L, Klumpers D, Darnell M, Bencherif S A, Weaver J C, Huebsch N, Lee H, Lippens E, Duda G N and Mooney D J 2016 Hydrogels with tunable stress relaxation regulate stem cell fate and activity *Nat Mater* **15** 326–34

[46] Mow V C, Kuei S C, Lai W M and Armstrong C G 1980 Biphasic creep and stress relaxation of articular cartilage in compression? Theory and experiments. *J. Biomech. Eng.* **102** 73–84

[47] Suh J K and Bai S 1998 Finite element formulation of biphasic poroviscoelastic model for articular cartilage. *J. Biomech. Eng.* **120** 195–201

[48] Li L P, Soulhat J, Buschmann M D and Shirazi-Adl A 1999 Nonlinear analysis of cartilage in unconfined ramp compression using a fibril reinforced poroelastic model *Clin. Biomech.* **14** 673–82

[49] Soltz M A and Ateshian G A 2000 Interstitial fluid pressurization during confined compression cyclical loading of articular cartilage. *Ann. Biomed. Eng.* **28** 150–9

[50] Li L P, Buschmann M D and Shirazi-Adl A 2003 Strain-rate dependent stiffness of articular cartilage in unconfined compression. *J. Biomech. Eng.* **125** 161–8

[51] Li L P, Buschmann M D and Shirazi-Adl A 2000 A fibril reinforced nonhomogeneous poroelastic model for articular cartilage: Inhomogeneous response in unconfined compression *J. Biomech.* **33** 1533–41

[52] Li L P, Korhonen R K, Iivarinen J, Jurvelin J S and Herzog W 2008 Fluid pressure driven fibril reinforcement in creep and relaxation tests of articular cartilage *Med. Eng. Phys.* **30** 182–9

[53] Gu K B and Li L P 2011 A human knee joint model considering fluid pressure and fiber orientation in cartilages and menisci *Med. Eng. Phys.* **33** 497–503

[54] Wong M, Ponticiello M, Kovanen V and Jurvelin J S 2000 Volumetric changes of articular cartilage during stress relaxation in unconfined compression. *J. Biomech.* **33** 1049–54

[55] Li L, Buschmann M D and Shirazi-Adl A 2002 The role of fibril reinforcement in the mechanical behavior of cartilage. *Biorheology* **39** 89–96

[56] Mow V C and Guo X E 2002 Mechano-electrochemical properties of articular cartilage: their inhomogeneities and anisotropies. *Annu. Rev. Biomed. Eng.* **4** 175–209

[57] Calvert P 2009 Hydrogels for Soft Machines *Adv. Mater.* **21** 743–56

[58] Wu T Y, Chwang A T, Teng M H and Valentine D T 2005 *Advances in Engineering Mechanics Reflections and Outlooks: In Honor of Theodore Y.-T. Wu* (World Scientific)

[59] Palmer A W, Guldberg R E and Levenston M E 2006 Analysis of cartilage matrix fixed charge density and three-dimensional morphology via contrast-enhanced

microcomputed tomography. *Proc. Natl. Acad. Sci. U. S. A.* **103** 19255–60

[60] Ateshian G A 2009 The role of interstitial fluid pressurization in articular cartilage lubrication *J. Biomech.* **42** 1163–76

[61] Mansour J M and Mow V C 1976 The permeability of articular cartilage under compressive strain and at high pressures *J. Bone Jt. Surg.* **58** 509–16

[62] Reynaud B and Quinn T M 2006 Anisotropic hydraulic permeability in compressed articular cartilage *J. Biomech.* **39** 131–7

[63] Bartnikowski M, Wellard R, Woodruff M and Klein T 2015 Tailoring Hydrogel Viscoelasticity with Physical and Chemical Crosslinking *Polymers (Basel).* **7** 2650–69

[64] Cameron A R, Frith J E, Gomez G A, Yap A S and Cooper-White J J 2014 The effect of time-dependent deformation of viscoelastic hydrogels on myogenic induction and Rac1 activity in mesenchymal stem cells *Biomaterials* **35** 1857–68

[65] McKinnon D D, Domaille D W, Cha J N and Anseth K S 2014 Biophysically defined and cytocompatible covalently adaptable networks as viscoelastic 3d cell culture systems *Adv. Mater.* **26** 865–72

[66] Jurvelin J S, Buschmann M D and Hunziker E B 2003 Mechanical anisotropy of the human knee articular cartilage in compression *Proc. Inst. Mech. Eng. Part H J. Eng. Med.* **217** 215–9

[67] Boschetti F, Pennati G, Gervaso F, Peretti G M and Dubini G 2004 Biomechanical properties of human articular cartilage under compressive loads. *Biorheology* **41** 159–66

[68] Athanasiou K A, Rosenwasser M P, Buckwalter J A, Malinin T I and Mow V C 1991 Interspecies comparisons of in situ intrinsic mechanical properties of distal femoral cartilage. *J. Orthop. Res.* **9** 330–40

[69] Athanasiou K A, Niederauer G G and Schenck R C 1995 Biomechanical topography of human ankle cartilage *Ann. Biomed. Eng.* **23** 697–704

[70] Athanasiou K A, Agarwal A and Dzida F J 1994 Comparative study of the intrinsic mechanical properties of the human acetabular and femoral head cartilage *J. Orthop. Res.* **12** 340–9

[71] Babuska I, Szabo B A, Katz I N and Mathematics A 1981 The p-Version of the Finite Element Method *SIAM J. Numer. Anal.* **18** 515–45

[72] Elder B D and Athanasiou K A 2009 Hydrostatic pressure in articular cartilage tissue engineering: from chondrocytes to tissue regeneration. *Tissue Eng. Part B. Rev.* **15** 43–53